# Ultrafast chiroptical switching in UV-excited molecules

Vincent Wanie[1*], Etienne Bloch[2], Erik P. Månsson[1], Lorenzo Colaizzi[1,3], Sergey Ryabchuk[3,4], Krishna Saraswathula[1,3], Andrea Trabattoni[1,5], Valérie Blanchet[2], Nadia Ben Amor[6], Marie-Catherine Heitz[6], Yann Mairesse[2], Bernard Pons[2*], Francesca Calegari [1, 3, 4]

[1] Center for Free-Electron Laser Science, Deutsches Elektronen-Synchrotron DESY, Notkestr. 85, 22607 Hamburg, Germany
[2] Université de Bordeaux - CNRS - CEA, CELIA, UMR5107, F-33405 Talence, France
[3] Physics Department, Universität Hamburg, Luruper Chaussee 149, 22761 Hamburg, Germany
[4]The Hamburg Centre for Ultrafast Imaging, Universität Hamburg, Luruper Chaussee 149, 22761 Hamburg, Germany
[5]Institute of Quantum Optics, Leibniz Universität Hannover, Welfengarten 1, 30167 Hannover, Germany
[6]CNRS, UPS, LCPQ (Laboratoire de Chimie et Physique Quantiques), FeRMI, 118 Route Narbonne, F-31062 Toulouse, France

**Imaging and manipulating the primary steps of transient chirality is key for controlling numerous physical, chemical and biological properties that arise from the chiral light-matter interaction. So far, the manifestation of electron-driven chiral dynamics has not been demonstrated at their natural timescale. Here, we use time-resolved photoelectron circular dichroism (TR-PECD) to image the dynamics of coherent electronic motion in neutral chiral molecules and disclose its impact on the molecular chiral response. We report on a rapid sign inversion of the chiroptical signal occurring in ~7 fs following the UV-excitation of methyl-lactate molecules. The populated electronic coherences can be used for chiroptical switching where the amplitude and direction of the net photoelectron current generated by PECD is controlled. The interpretation of the results is supported by theoretical modelling of both the molecular photoexcitation to Rydberg states and the subsequent photoionization via PECD. Our findings establish a general method to investigate electron dynamics in a variety of chiral systems with high sensitivity and pave the way to a new scheme for enantio-sensitive charge-directed reactivity in neutral chiral molecules.**

Chirality is a peculiar property that characterizes the majority of biochemical systems: a chiral molecule exists in two geometrical configurations that are non-superimposable mirror images of each other - defined as (*R)* and (*S)* enantiomers - exhibiting different physical and chemical properties when interacting with another chiral entity. This chiral recognition is central to many fields of applied sciences, including enantioselective catalysis, drug engineering and biophysics (*1*, *2*).

Capturing the primary steps of chiral recognition and the mechanisms dictating the outcomes of a chiral interaction would thus have a significant impact in various fields working with chiral property of matter. At the ultrafast electronic timescale for instance, the opportunity to steer electrons responsible for chemical activity notably promises a way to control the outcome of enantio-sensitive reactions (*3*) via charge-directed reactivity (*4–6*). However, the ability to track and control electron-driven chiral interactions as well as other electron dynamics in biochemically-relevant neutral molecules in general remains to be demonstrated.

In this context, the temporal resolution provided by attosecond technologies developed in the past twenty years gives access to the fastest electron dynamics of matter on their natural timescale. Seminal pump-probe experiments using attosecond light pulses have revealed valence electron dynamics in atoms (*7*), autoionization dynamics in molecules (*8*), photoionization delays in solids (*9*, *10*) as well as electron-driven charge migration in biomolecules (*6*, *11*). However, the intrinsically high photon energy of attosecond light sources inevitably leads to target ionization, which results in probing ultrafast dynamics of cationic states. Investigating the light-induced electron dynamics of biochemically-relevant

neutral molecules with high temporal resolution requires new experimental approaches. Two important technological challenges must be addressed. First, the pump pulse must have well-defined characteristics: (i) a photon energy below the ionization threshold, (ii) a broadband energy spectrum to trigger electron motion among multiple electronic states and (iii) a time duration that provides a prompt excitation before any nuclear motion can take place, together with sufficient temporal resolution. Because of the low ionization potential of most molecular systems, laser pulses with such characteristics are confined to a narrow spectral region covering the ultraviolet (UV) and the vacuum-UV ranges, which also avoid triggering complex high-order, strong-field multiphoton driven processes that typically do not occur in nature (*12*).

Second, the spectroscopic observable must be carefully chosen. In other words, how to probe electron dynamics with an increased sensitivity compared to typical ultrafast spectroscopic methods such as all-optical transient absorption spectroscopy or time-resolved photoelectron and photoion spectroscopies (*13*, *14*)? Since light can be imprinted with a chiral character when circularly polarized, a promising approach is to use the chiroptical response of bio-relevant systems to investigate their ultrafast dynamics.

It is known since 1976 that the photoionization of randomly oriented chiral molecules by circularly polarized radiation yields a photoelectron angular distribution (PAD) which presents a forward-backward asymmetry along the light propagation axis (*15*, *16*). This asymmetry, referred to as PhotoElectron Circular Dichroism (PECD), is orders of magnitude larger than the conventional absorption circular dichroism (*17*), and it is therefore well suited to the study of chiral features in the gas phase. PECD was shown to be strongly sensitive to a wealth of structural molecular properties, including the nature of ionized

orbitals and continuum states (*18*), isomerism and chemical substitution (*19*, *20*) and the vibrational structure of the cation (*21*). While structural features are generally gained from static measurements, the availability of femtosecond and attosecond pulses provides a valuable tool to characterize and manipulate the dynamical properties of chiral neutral molecules at the electron timescale. So far, the strength of this method has only been demonstrated in the time domain for the investigation of nuclear dynamics, internal conversion and photoionization delays in chiral molecules (*22*–*25*).

Here, we employ a novel laser-based technology delivering few-femtosecond UV pulses (*26*) to perform TR-PECD measurements with unprecedented temporal resolution and extend the method to the investigation of electron-driven chiral interactions in neutral methyl-lactate (ML) – a derivative of lactate, which has regained substantial interest due to its recently uncovered metabolic functions (*27*). A linearly polarized UV pulse promptly launches a coherent electronic wavepacket in the bio-relevant molecule while a time-delayed circularly polarized near-infrared (NIR) probe triggers ionization from the transient wavepacket (Fig.1a). The chiroptical molecular response is characterized by the preferential direction of emission of the ejected electron through PECD. Numerical simulations modelling the experiment show that the NIR pulse tracks electronic beatings initiated by the coherent superposition of Rydberg states created by the broadband UV pump pulse. The resulting oscillations of the charge density can be used for chiroptical switching in which the net photoelectron current from the initially isotropic sample is reversed on a sub-10 fs timescale when adjusting the pump-probe time delay.

Fig. 1 shows an overview of the experimental approach used to investigate in real-time the chiral dynamics of ML. Following sudden photoexcitation of (*S*)-ML enantiomers just below the ionization threshold by a few-fs UV pulse, a circularly polarized near-infrared (NIR) probe pulse leads to photoionization (a). For each pump-probe delay $t$, the photoelectron angular distributions (PADs) are collected with a velocity map imaging spectrometer (VMIs) for both left ($h=+1$) and right ($h=-1$) circular polarizations of the NIR probe pulse. These raw distributions are then fitted using a pBasex inversion algorithm (see section 1.2 of the supplement) (*22*) to yield the PAD $S^{(h)}(\epsilon,\theta,t)$, where $\epsilon$ is the kinetic energy of the photoelectron and $\theta$ its emission angle with respect to the light propagation axis. The differential PECD image is then defined as the normalized difference $PECD(\epsilon,\theta,t)=2\frac{S^{(+1)}(\epsilon,\theta,t)-S^{(-1)}(\epsilon,\theta,t)}{S^{(+1)}(\epsilon,\theta,t)+S^{(-1)}(\epsilon,\theta,t)}$ and its evolution is observed as a function of the pump-probe delay $t$. Figure 1b displays $PECD(\epsilon,\theta,t)$ for $t=5,11,17$ and $26$ fs, which captures an inversion of the photoelectron forward-backward asymmetry in about $7$ fs.

The inversion procedure consists in fitting the VMIs images according to $S^{(h)}(\epsilon,\theta,t)=\sum_{n=0}^{2N} b_n^{(h)}(\epsilon,t)P_n(\cos\theta)$ where $P_n(\cos\theta)$ are Legendre polynomials and $N=3$ is the total number of photons absorbed to reach the continuum from the ground state: the pump-induced excitation involves 2 photons while ionization consists in the absorption of one NIR probe photon. $b_0^{(h)}(\epsilon,t)$ corresponds to the total (angle-integrated) photoionization cross section. In the case of an achiral sample, the PAD is symmetric with respect to the light propagation axis so that the $S^{(h)}(\epsilon,\theta,t)$ expansion is restricted to even *n*'s. For chiral

samples, the asymmetric contribution to the photoelectron yield emerges from the additional $b_n^{(h)}$ amplitude coefficients with odd $n$. Besides $PECD(\epsilon,\theta,t)$, it is convenient to introduce an angularly-integrated quantity to characterize the whole chiroptical response at fixed kinetic energy. Defining it as the difference of electrons emitted in the forward and backward hemispheres for $h=+1$, normalized to the average number of electrons collected in one hemisphere, we obtain the so-called multiphotonic (MP)-PECD (*28*),

$$MP-PECD(\epsilon,t)=2\beta_1^{(+1)}(\epsilon,t)-\frac{1}{2}\beta_3^{(+1)}(\epsilon,t)+\frac{1}{4}\beta_5^{(+1)}(\epsilon,t) \text{ where } \beta_n^{(+1)}(\epsilon,t)=\frac{b_n^{(+1)}(\epsilon,t)}{b_0^{(+1)}(\epsilon,t)}.$$

In our analysis the $b_5$ coefficient has been omitted due to its negligible contribution. Figure 2 shows the multiphotonic PECD as a function of the delay $t$ for three $\epsilon$ ranges defined by the time- and energy-resolved map of the $\beta_1^{\square}(\epsilon,t)$ coefficient (see Fig. S2d of the supplement). The results are shown for (*S*)-ML but the measurements were also performed in (*R*)-ML – the comparison of enantiomeric responses is shown in Fig. S4 of the supplement. For the lowest $\epsilon$ range between 25-100 meV (a), it is striking that the photoelectron emission asymmetry reverses in the laboratory frame in ~7 fs. A clear modulation of the asymmetry remains over few tens of fs, which is also observed at higher $\epsilon$ between 100-300 meV (b) and 300-720 meV (c). Importantly, such a clear modulation hardly shows up in the time-resolved $\beta_0^{\square}(\epsilon,t)$ coefficient associated to the photoelectron yield (see Section 1.2 of the supplement). This latter observable provides a limited signal to noise ratio compared to the odd coefficients $\beta_{2n+1}^{\square}(\epsilon,t)$evaluated from differential measurements, highlighting the capabilities of TR-PECD over conventional photoelectron spectroscopy. In the following, we aim at identifying the origin of the modulation, taking into account that the timescale possibly involves electronic and/or nuclear degrees of freedom.

We modeled the experiment including both the UV photoexcitation and the NIR photoionization steps. A detailed description of the theoretical method is provided in Section 2 of the supplement. Briefly, we treat the photoexcitation and photoionization as sequential perturbative processes. The electronic spectrum of ML and the two-photon excitation amplitudes are obtained via large-scale time-dependent density functional theory. Ionization from the excited states is described using the continuum multiple scattering X$\alpha$ approach. Importantly, we work within the frozen-nuclei approximation.

We illustrate the results of our calculations in Figure 3. The two-photon excitation cross sections is presented in panel (a), including states with a HOMO (red) or HOMO-1 (green) orbital character of at least 60%. For the calculations, we emphasize on the states associated to almost pure HOMO excitation ≥80% shown by the red filled dots, from which photoionization by the probe profile (Gaussian curves) can subsequently lead to the emission of photoelectrons with kinetic energies $\epsilon = 250$ and $500$ meV, respectively. These $\epsilon$ values are representative of the second and third energy ranges discriminated in the experimental data, respectively – the case of low energy photoelectron dynamics ($\epsilon = 50$ meV) is discussed in Section 2.2.3 of the supplement. Including the HOMO excited states in the dynamical calculations yield the time-resolved MP-PECD displayed in panels (b) and (d). The asymmetry presents clear modulations as a function of the pump-probe delay. The power spectra of the MP-PECD signals, obtained by Fourier analysis, are compared to their experimental counterparts in panels (c) and (e). An excellent agreement is found at $\epsilon$ = 250 meV where the oscillatory pattern of the MP-PECD is traced back to the pump-induced coherent superposition of 3d and 4p Rydberg states highlighted in Figure 3(a). This coherent superposition leads to quantum beatings with 15 fs period, associated to

300 meV frequency, which survive long after the pump pulse vanishes. We note that the most stable geometries of methyl-lactate do not possess any vibrational mode in the vicinity of 2200 $cm^{-1}$ (~15 fs) (*29*). Similarly, the coherent superposition of 4p and 4d,f Rydberg states explains the oscillatory feature of the MP-PECD at $\epsilon$ = 500 meV. A small mismatch of 60 meV is observed between the experimental and theoretical power spectra in Figure 3(e). This is typical of the error made in quantum chemistry computations of excited state energies.

In our fixed-nuclei description, the electron coherences leading to oscillatory MP-PECD do not vanish. In the experiments, they are found to decrease as time elapses, through decreasing MP-PECD amplitudes (Figure 2), but are preserved on a relatively long timescale, up to ~40 fs. The time it takes for decoherence to occur in photoionized (*30*–*37*) and photoexcited (*12*, *38*) molecules is currently the subject of extensive investigations. Electronic wavepackets are subject to three main decoherence sources: (i) the decrease of the overlap between nuclear wavepackets on different electronic states, (ii) the dephasing of the different wavepacket components, and (iii) the change of electronic state populations induced by non-adiabatic couplings (*32*). Describing the coupled electron and nuclear dynamics in an energy range with tens of electronic states (see Figure S11 of the supplement) is beyond state-of-the-art theoretical approaches. Therefore, we alternatively performed classical molecular dynamics calculations on the ground state of cationic ML to which all the HOMO Rydberg states involved in the pump-probe dynamics correlate upon ionization. Two main classes of trajectories showed up, converging towards two different isomeric forms of the ML cation. Within each class of trajectories, the Rydberg state

energies of neutral ML were found to remain approximately parallel to each other and to the ML cation along the reaction path (see Figure S11 of the supplement). This favors the overlap of the nuclear wavepackets on the electronic Rydberg states over an extended time duration and thus minimizes the role of mechanisms (i) and (ii) for decoherence. This also strengthens the frozen-nuclei assumption with regard to the description of electronic quantum beatings which are dictated by energy differences and should therefore remain basically the same from $t=0$ onwards. The most probable source of decoherence in the present investigation is non-adiabatic dynamics, not only between the states populated by the pump but also with the lower-lying states reached by internal conversion soon after the prompt excitation. This information is encoded in the ~40 fs lifetime of the transient $b_0$ signal (see Fig. S3 of the supplement).

Our findings on fast evolving MP-PECD and related chiroptical switching, driven by long-lasting electronic coherences, can be highlighted by reducing the number of transient excited states to two. In the case of $\epsilon$ = 250 meV, the main MP-PECD oscillation frequency is 291 meV and corresponds to the coherent superposition of the 3d and 4p Rydberg states, respectively located at $E_{3d}=8.834$ eV and $E_{4p}=9.120$ eV on the energy scale (Fig. 3a). For a single molecular orientation $\hat{R}$, the excited electron wavepacket thus reads, at time $t$ after the pump pulse vanishes, $\Phi(\hat{R},r,t)=\sum_{j=3d,4p} A_j(\hat{R})\,\Psi_j(r)\exp(-i\,E_j t/\hbar)$ where $A_i(\hat{R})$ are the two-photon transition amplitudes associated to the excited states $\Psi_j(r)$. The associated electron density can be partitioned as

$$\rho(\hat{R},r,t)=\rho_{incoh}(\hat{R},r)+\rho_{cross}(\hat{R},r)\cos\left[(E_{4p}-E_{3d})t/\hbar\right] \qquad (1)$$

where $\rho_{incoh}(\hat{R},r)=A_{3d}^2(\hat{R})\Psi_{3d}^2(r)+A_{4p}^2(\hat{R})\Psi_{4p}^2(r)$, with $\hat{R}$ such that $A_i(\hat{R})\in R$, and $\rho_{cross}(\hat{R},r)=2A_{3d}^{\square}(\hat{R})A_{4p}^{\square}(\hat{R})\Psi_{3d}^{\square}(r)\Psi_{4p}^{\square}(r)$. Figure 4(a) shows the coherent part $\rho(\hat{R},r,t)-\rho_{incoh}(\hat{R},r)$ of the electron density, oscillating back-and-forth along the molecular structure with a period $T=2\pi\hbar/(E_{4p}-E_{3d})$ of 14.4 fs. Ionization of the 3d and 4p state superposition leads, after averaging over the orientations $\hat{R}$, to the total photoelectron yield which can be decomposed similarly to (1):

$$b_0^{(\pm1)}(\epsilon,t)=b_{0_{incoh}}^{(\pm1)}(\epsilon)+b_{0_{cross}}^{(\pm1)}(\epsilon)\cos\left[(E_{4p}-E_{3d})t/\hbar\right]. \qquad (2)$$

The computed yield is presented in Figure 4(b) for $\epsilon=250$meV, showing how the coherent state superposition leading to $b_{0_{cross}}^{(\pm1)}(\epsilon)\cos\left[(E_{4p}-E_{3d})t/\hbar\right]$modulates the incoherent sum $b_{0_{incoh}}^{(\pm1)}(\epsilon)$ of individual cross sections. The unnormalized MP-PECD can in turn be written as:

$$MP\text{-}PECD(\epsilon,t)=MP\text{-}PECD_{incoh}(\epsilon)+MP\text{-}PECD_{cross}(\epsilon)\cos\left[\frac{(E_{4p}-E_{3d})t}{\hbar}-\Delta\phi\right] \qquad (3)$$

where the additional phase $\Delta\phi$ arises from the interference of the state-selective continuum partial wave amplitudes building the asymmetry of the photoelectron yield (see the supplement) – as usual, this interference is washed out at the level of the total photoelectron yield (*39*, *40*). The temporal evolution of the unnormalized two-state MP-PECD is shown in Figure 4(c) from which we extract the time delay$\Delta t=1.8$ fs associated to $\Delta\phi=0.79$ rad. The MP-PECD reverses sign within our period of the oscillation since the asymmetries of single 3d- and 4p-mediated pathways, contributing to the incoherent MP-PECD (dashed red line in Fig. 4c) around which the coherent part oscillates, are opposite for $\epsilon=250$meV. Such a chiroptical switching depends not only on the transient bound resonances but also on the dichroism encoded by ionization. In this respect, we note that a

photoexcitation electron circular dichroism configuration (*41*) in which molecules are photoexcited by a circularly polarized pump pulse and subsequently ionized with a linearly polarized probe would reduce the degrees of freedom to only the transient bound resonances. (*41*)

In conclusion, we have shown how the prompt creation of an electronic wavepacket by a few-fs UV pulse dictates the chiral properties of methyl-lactate in the first instants following photoexcitation, allowing for ultrafast chiroptical switching. The high sensitivity of TR-PECD that allows us to track electronic coherences is intrinsic to its differential, background-free nature. A complete modelling of the experiment identifies how the chiral character of Rydberg states contributes to chiroptical switching and additional trajectory calculations describe how the electron dynamics driving the effect can preserve the coherence over several tens of femtoseconds. The experimental results demonstrate that our spectroscopic method can provide insights on the sub-vibrational nature of chiral interactions at the few-fs timescale, notably the role of the primary electron dynamics in the light-induced chiral response of molecular systems with increasing complexity such as chiral biomolecules and organometallic complexes. Offering a route to investigate the fundamental origin of chiral recognition that is ubiquitous in biological phenomena (*42*), the possibility to control the photoelectron emission direction in the laboratory frame also offers the potential to engineer petahertz switching devices based on chiral interactions. Most importantly, these results provide new perspectives towards the possibility to achieve enantio-sensitive charge-directed reactivity in neutral molecules to steer the outcome of chemical reactions (*3*).

## ACKNOWLEDGEMENTS

We thank K. Pikull for the excellent technical support.

## FUNDING

We acknowledge financial support from the European Research Council under the ERC-2014-StG STARLIGHT (grant no. 637756), European Union's Horizon 2020 research and innovation program No. 682978 – EXCITERS, the German Research Foundation (DFG)—SFB-925—project 170620586 and the Cluster of Excellence Advanced Imaging of Matter (AIM).

## AUTHOR CONTRIBUTIONS

V.W., E.B., V.B., Y.M., B.P. and F.C. conceived the experiment. V.W., E.B., E.P.M., L.C., S.R., K.S. and A.T. performed the experiments. V.W., E.B. and Y.M., carried out the data analysis. M.C.H., N.B.A. and B.P. calculated the molecular and electronic properties of methyl-lactate. B.P. performed the PECD calculations. M.C.H. performed the classical trajectory simulations. V.W., Y.M., B.P. and F.C. drafted the manuscript. All authors contributed to the discussion of the results and the editing of the manuscript.

## DATA AVAILABILITY

The data that support the findings of this study are available from the corresponding author upon reasonable request.

## CODE AVAILABILITY

The code used for the simulations contained in this study is available from the corresponding authors upon reasonable request.

## COMPETING INTERESTS

The authors declare no competing interests.

## References

1. Jochen R. Brandt, Francesco Salerno, Matthew J. Fuchter, The added value of small-molecule chirality in technological applications. *Nat Rev Chem*. **1** (2017) (available at www.nature.com/natrevchem).
2. B. L. Feringa, R. A. van Delden, N. Koumura, E. M. Geertsema, Chiroptical Molecular Switches. *Chem Rev*. **100**, 1789–1816 (2000).
3. A. F. Ordonez, D. Ayuso, P. Decleva, O. Smirnova, Geometric fields and new enantio-sensitive observables in photoionization of chiral molecules (2021) (available at http://arxiv.org/abs/2106.14264).
4. R. Weinkauf, E. W. Schlag, T. J. Martinez, R. D. Levine, "Nonstationary Electronic States and Site-Selective Reactivity" (1997), (available at https://pubs.acs.org/sharingguidelines).

5. F. Remacle, R. D. Levine, An electronic time scale in chemistry. *Proc Natl Acad Sci U S A*. **103**, 6793–6798 (2006).
6. E. P. Månsson, S. Latini, F. Covito, V. Wanie, M. Galli, E. Perfetto, G. Stefanucci, H. Hübener, U. de Giovannini, M. C. Castrovilli, A. Trabattoni, F. Frassetto, L. Poletto, J. B. Greenwood, F. Légaré, M. Nisoli, A. Rubio, F. Calegari, Real-time observation of a correlation-driven sub 3 fs charge migration in ionised adenine. *Commun Chem*. **4** (2021), doi:10.1038/s42004-021-00510-5.
7. E. Goulielmakis, Z. H. Loh, A. Wirth, R. Santra, N. Rohringer, V. S. Yakovlev, S. Zherebtsov, T. Pfeifer, A. M. Azzeer, M. F. Kling, S. R. Leone, F. Krausz, Real-time observation of valence electron motion. *Nature*. **466**, 739–743 (2010).
8. S. Haessler, B. Fabre, J. Higuet, J. Caillat, T. Ruchon, P. Breger, B. Carré, E. Constant, A. Maquet, E. Mével, P. Salières, R. Taïeb, Y. Mairesse, Phase-resolved attosecond near-threshold photoionization of molecular nitrogen. *Phys Rev A (Coll Park)*. **80**, 011404 (2009).
9. A. L. Cavalieri, N. Müller, T. Uphues, V. S. Yakovlev, A. Baltuska, B. Horvath, B. Schmidt, L. Blümel, R. Holzwarth, S. Hendel, M. Drescher, U. Kleineberg, P. M. Echenique, R. Kienberger, F. Krausz, U. Heinzmann, Attosecond spectroscopy in condensed matter. *Nature*. **449**, 1029–1032 (2007).
10. M. Schultze, M. Fieß, N. Karpowicz, J. Gagnon, M. Korbman, M. Hofstetter, S. Neppl, A. L. Cavalieri, Y. Komninos, T. Mercouris, C. A. Nicolaides, R. Pazourek, S. Nagele, J. Feist, J. Burgdörfer, A. M. Azzeer, R. Ernstorfer, R. Kienberger, U. Kleineberg, E. Goulielmakis, F. Krausz, V. S. Yakovlev, Delay in photoemission. *Science (1979)*. **328**, 1658–1662 (2010).
11. F. Calegari, D. Ayuso, A. Trabattoni, L. Belshaw, S. de Camillis, S. Anumula, F. Frassetto, L. Poletto, A. Palacios, P. Decleva, J. B. Greenwood, F. Martín, M. Nisoli, Ultrafast electron dynamics in phenylalanine initiated by attosecond pulses. *Science (1979)*. **346**, 336–339 (2014).
12. D. T. Matselyukh, V. Despré, N. v. Golubev, A. I. Kuleff, H. J. Wörner, Decoherence and revival in attosecond charge migration driven by non-adiabatic dynamics. *Nat Phys* (2022), doi:10.1038/s41567-022-01690-0.
13. T. Suzuki, B. J. Whitaker, Non-adiabatic effects in chemistry revealed by time-resolved charged-particle imaging. *Int Rev Phys Chem*. **20** (2001), pp. 313–356.
14. R. Geneaux, H. J. B. Marroux, A. Guggenmos, D. M. Neumark, S. R. Leone, Transient absorption spectroscopy using high harmonic generation: A review of ultrafast X-ray dynamics in molecules and solids. *Philosophical Transactions of the Royal Society A: Mathematical, Physical and Engineering Sciences*. **377** (2019), , doi:10.1098/rsta.2017.0463.
15. B. Ritchie, Theory of the angular distribution for ejection of photoelectrons from optically active molecules and molecular negative ions. II. *Phys Rev A (Coll Park)*. **14**, 359–362 (1976).
16. N. Böwering, T. Lischke, B. Schmidtke, N. Müller, T. Khalil, U. Heinzmann, Asymmetry in photoelectron emission from chiral molecules induced by circularly polarized light. *Phys Rev Lett*. **86**, 1187–1190 (2001).
17. S. Daly, I. Powis, G. A. Garcia, H. Soldi-Lose, L. Nahon, Photoionization of epichlorohydrin enantiomers and clusters studied with circularly polarized vacuum ultraviolet radiation. *Journal of Chemical Physics*. **134** (2011), doi:10.1063/1.3536500.
18. L. Nahon, G. A. Garcia, C. J. Harding, E. Mikajlo, I. Powis, Determination of chiral asymmetries in the valence photoionization of camphor enantiomers by photoelectron imaging using tunable circularly polarized light. *Journal of Chemical Physics*. **125**, 114309 (2006).

19. G. A. Garcia, H. Dossmann, L. Nahon, S. Daly, I. Powis, Photoelectron circular dichroism and spectroscopy of trifluoromethyl- and methyl-oxirane: A comparative study. *Physical Chemistry Chemical Physics*. **16**, 16214–16224 (2014).
20. I. Powis, C. J. Harding, G. A. Garcia, L. Nahon, A valence photoelectron imaging investigation of chiral asymmetry in the photoionization of fenchone and camphor. *ChemPhysChem*. **9**, 475–483 (2008).
21. G. A. Garcia, L. Nahon, S. Daly, I. Powis, Vibrationally induced inversion of photoelectron forward-backward asymmetry in chiral molecule photoionization by circularly polarized light. *Nat Commun*. **4**, 1–6 (2013).
22. A. Comby, S. Beaulieu, M. Boggio-Pasqua, D. Descamps, F. Légaré, L. Nahon, S. Petit, B. Pons, B. Fabre, Y. Mairesse, V. Blanchet, Relaxation Dynamics in Photoexcited Chiral Molecules Studied by Time-Resolved Photoelectron Circular Dichroism: Toward Chiral Femtochemistry. *Journal of Physical Chemistry Letters*. **7**, 4514–4519 (2016).
23. S. Beaulieu, A. Comby, A. Clergerie, J. Caillat, D. Descamps, N. Dudovich, B. Fabre, R. Géneaux, F. Légaré, S. Petit, B. Pons, G. Porat, T. Ruchon, R. Täieb, V. Blanchet, Y. Mairesse, Attosecond-resolved photoionization of chiral molecules. *Science (1979)*. **358**, 1288–1294 (2017).
24. V. Blanchet, D. Descamps, S. Petit, Y. Mairesse, B. Pons, B. Fabre, Ultrafast relaxation investigated by photoelectron circular dichroism: an isomeric comparison of camphor and fenchone. *Physical Chemistry Chemical Physics* (2021), doi:10.1039/d1cp03569j.
25. V. Svoboda, N. Bhargava Ram, D. Baykusheva, D. Zindel, M. D. J Waters, B. Spenger, M. Ochsner, H. Herburger, J. Stohner, H. Jakob Wörner, "Femtosecond photoelectron circular dichroism of chemical reactions" (2022), (available at https://www.science.org).
26. M. Galli, V. Wanie, D. P. Lopes, E. P. Månsson, A. Trabattoni, L. Colaizzi, K. Saraswathula, A. Cartella, F. Frassetto, L. Poletto, F. Légaré, S. Stagira, M. Nisoli, R. Martínez Vázquez, R. Osellame, F. Calegari, Generation of deep ultraviolet sub-2-fs pulses. *Opt Lett*. **44**, 1308 (2019).
27. G. A. Brooks, J. A. Arevalo, A. D. Osmond, R. G. Leija, C. C. Curl, A. P. Tovar, Lactate in contemporary biology: a phoenix risen. *Journal of Physiology*. **600**, 1229–1251 (2022).
28. C. S. Lehmann, N. B. Ram, I. Powis, M. H. M. Janssen, Imaging photoelectron circular dichroism of chiral molecules by femtosecond multiphoton coincidence detection. *Journal of Chemical Physics*. **139** (2013), doi:10.1063/1.4844295.
29. A. Borba, A. Gómez-Zavaglia, L. Lapinski, R. Fausto, Matrix isolation FTIR spectroscopic and theoretical study of methyl lactate. *Vib Spectrosc*. **36**, 79–88 (2004).
30. M. Vacher, L. Steinberg, A. J. Jenkins, M. J. Bearpark, M. A. Robb, Electron dynamics following photoionization: Decoherence due to the nuclear-wave-packet width. *Phys Rev A*. **92** (2015), doi:10.1103/PhysRevA.92.040502.
31. C. Arnold, O. Vendrell, R. Santra, Electronic decoherence following photoionization: Full quantum-dynamical treatment of the influence of nuclear motion. *Phys Rev A (Coll Park)*. **95** (2017), doi:10.1103/PhysRevA.95.033425.
32. M. Vacher, M. J. Bearpark, M. A. Robb, J. P. Malhado, Electron Dynamics upon Ionization of Polyatomic Molecules: Coupling to Quantum Nuclear Motion and Decoherence. *Phys Rev Lett*. **118** (2017), doi:10.1103/PhysRevLett.118.083001.
33. C. Arnold, O. Vendrell, R. Welsch, R. Santra, Control of Nuclear Dynamics through Conical Intersections and Electronic Coherences. *Phys Rev Lett*. **120** (2018), doi:10.1103/PhysRevLett.120.123001.

34. N. v. Golubev, T. Begušić, J. Vaníček, On-the-Fly Ab Initio Semiclassical Evaluation of Electronic Coherences in Polyatomic Molecules Reveals a Simple Mechanism of Decoherence. *Phys Rev Lett*. **125** (2020), doi:10.1103/PhysRevLett.125.083001.
35. V. Despré, N. v. Golubev, A. I. Kuleff, Charge Migration in Propiolic Acid: A Full Quantum Dynamical Study. *Phys Rev Lett*. **121** (2018), doi:10.1103/PhysRevLett.121.203002.
36. V. Despré, A. Marciniak, V. Loriot, M. C. E. Galbraith, A. Rouzée, M. J. J. Vrakking, F. Lépine, A. I. Kuleff, Attosecond hole migration in benzene molecules surviving nuclear motion. *Journal of Physical Chemistry Letters*. **6**, 426–431 (2015).
37. M. Lara-Astiaso, A. Palacios, P. Decleva, I. Tavernelli, F. Martín, Role of electron-nuclear coupled dynamics on charge migration induced by attosecond pulses in glycine. *Chem Phys Lett*. **683**, 357–364 (2017).
38. A. Csehi, P. Badankó, G. J. Halász, Á. Vibók, B. Lasorne, On the preservation of coherence in the electronic wavepacket of a neutral and rigid polyatomic molecule. *Journal of Physics B: Atomic, Molecular and Optical Physics*. **53** (2020), doi:10.1088/1361-6455/aba10e.
39. D. Dill, J. L. Dehmer, Electron-molecule scattering and molecular photoionization using the multiple-scattering method. *J Chem Phys*. **61**, 692–699 (1974).
40. I. Powis, "PHOTOELECTRON CIRCULAR DICHROISM IN CHIRAL MOLECULES" in *Advances in Chemical Physics*, S. A. Rice, Ed. (2008; https://onlinelibrary.wiley.com/doi/abs/10.1002/9780470259474.ch5), vol. 138, pp. 267–329.
41. S. Beaulieu, A. Comby, D. Descamps, B. Fabre, G. A. Garcia, R. Géneaux, A. G. Harvey, F. Légaré, Z. Mašín, L. Nahon, A. F. Ordonez, S. Petit, B. Pons, Y. Mairesse, O. Smirnova, V. Blanchet, Photoexcitation circular dichroism in chiral molecules. *Nat Phys*. **14**, 484–489 (2018).
42. A. Zehnacker, M. A. Suhm, Chirality recognition between neutral molecules in the gas phase. *Angewandte Chemie - International Edition*. **47**, 6970–6992 (2008).

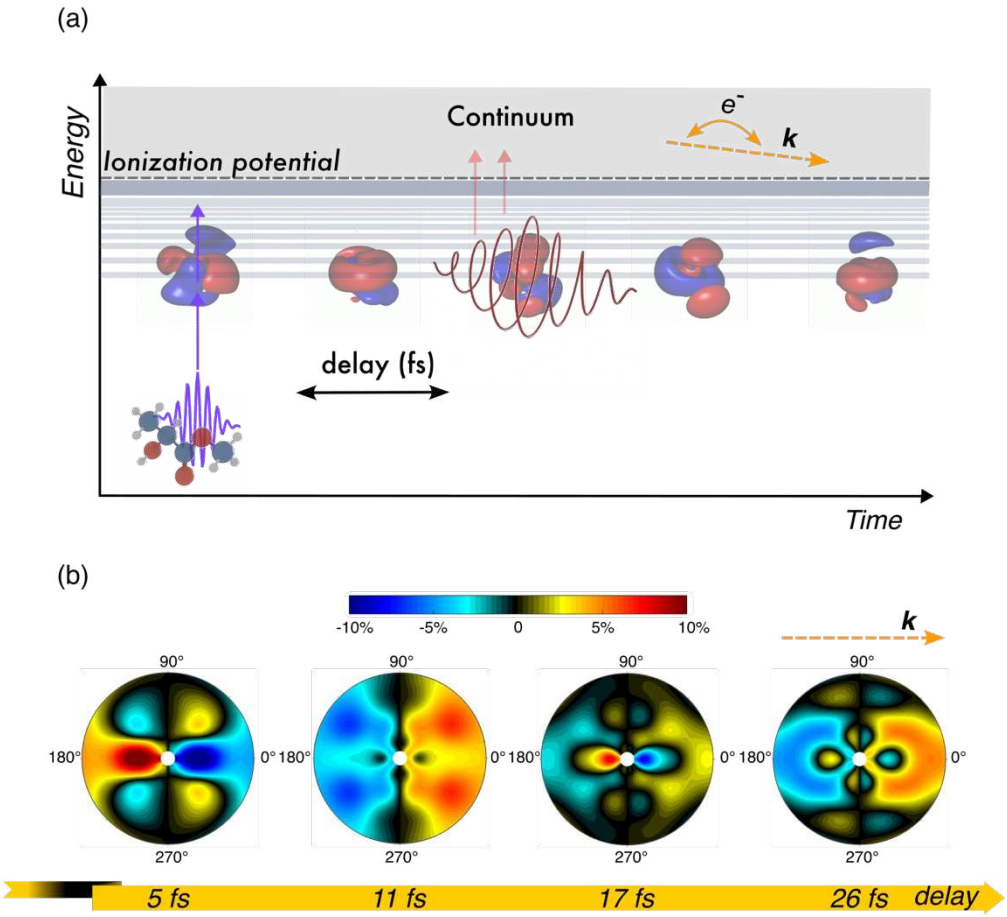


Fig. 1: **Light-induced chiral dynamics of methyl-lactate.** (a) A few-femtosecond linearly polarized UV pulse creates an electronic wavepacket of Rydberg states via 2-photon absorption. A time-delayed, circularly polarized NIR pulse probes the the transient electronic wavepacket in the neutral molecule via the ejection of an electron along the light propagation axis defined by the vector *k*. The large bandwidth of the probe pulse allows two or more Rydberg states to reach the same electron continuum state and thus probe their interference. (b) The resulting photoelectron angular distribution is recorded by a velocity map imaging spectrometer. For each time delay, an image is recorded for both left (LCP) and right circular polarization (RCP) of the probe pulse. The differential image (LCP - RCP), normalized by the average signal and subsequently inverted, is shown for time delays of 5, 11,17 and 26 fs for photoelectrons with kinetic energies from 25 to 300 meV along the radial coordinate.

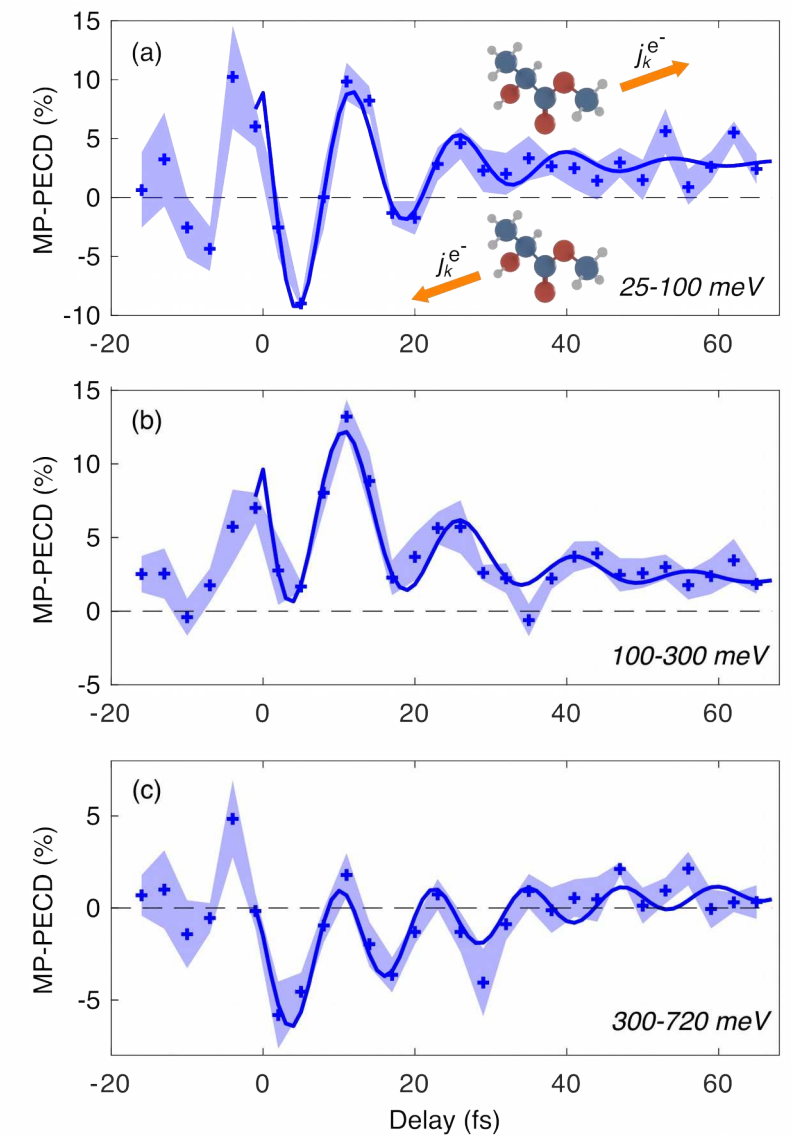


Fig. 2: **Energy-resolved analysis.** Temporal evolution of the MP-PECD in (*S*) - methyl-lactate for three different kinetic energy ranges of photoelectrons: 25-100 meV (a), 100-300 meV (b) and 300-720 meV (c). The standard error of the mean over 5 measurements is shown by the shaded areas and the solid blue lines show the fit of the oscillations from $t = 0$ fs (see the corresponding Fourier analysis in Fig. 3d,e). The change of sign in (a) identifies a reversal of the photoelectron emission direction in the laboratory frame, generating a net photoelectron current $j_k^{e^-}$ along the light propagation direction *k*.

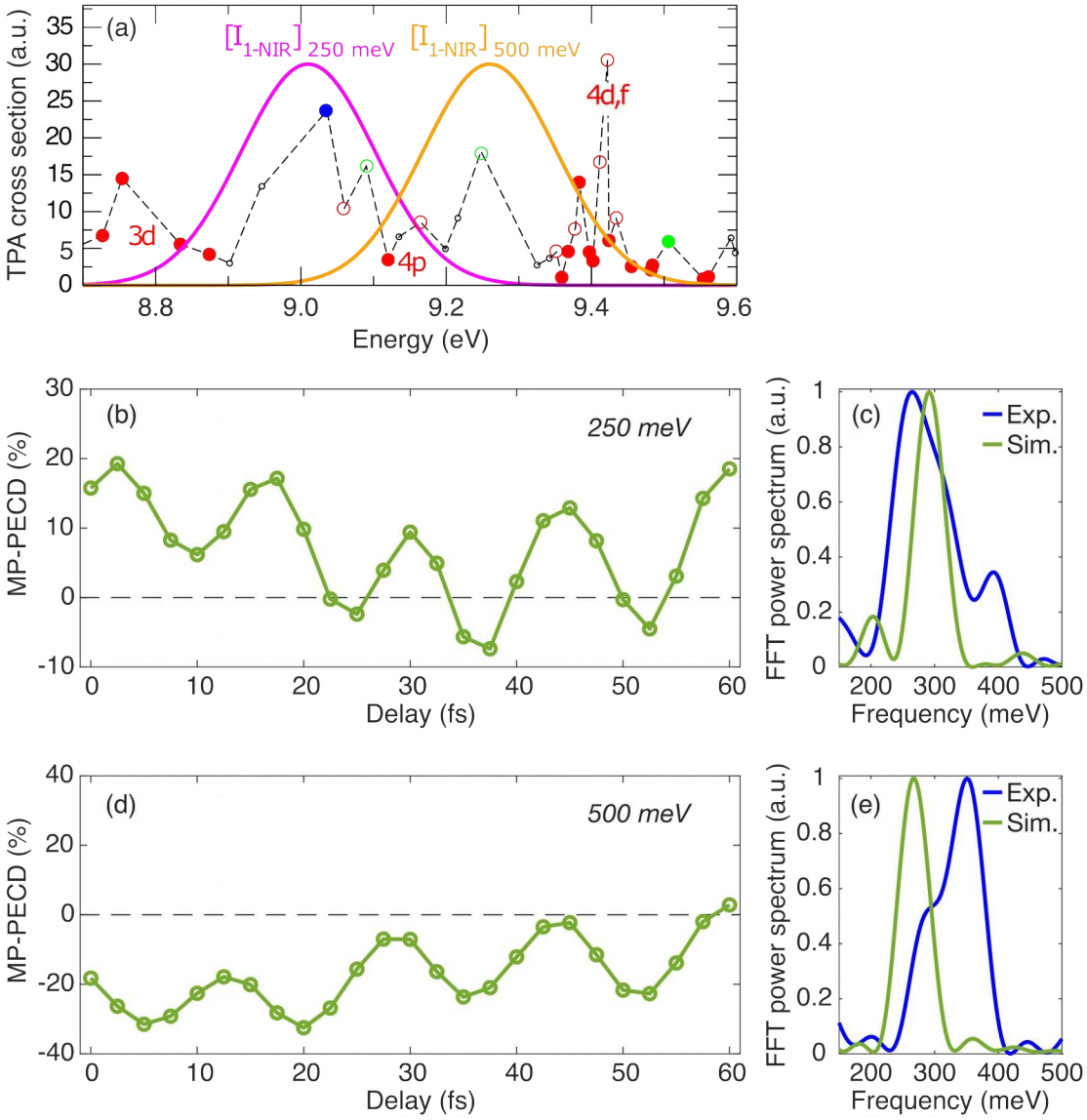


Fig. 3: **Modelling of the experiment.** (a) Two-photon absorption (TPA) cross sections for HOMO and HOMO-1 excitation convoluted with the the UV-pump intensity squared. The red and green filled circles emphasize the excited states stemming from HOMO and HOMO-1 excitations >80% respectively. The magenta and orange curves correspond to the spectral probe intensity, down-shifted in energy to elicit the transient Rydberg states leading to photoelectrons with energies $\epsilon = 250$ and $\epsilon = 500$ meV through ionization by one photon centred at frequency $\omega = 1.75$ eV. (b) Calculated MP-PECD for photoelectrons with $\epsilon = 250$ meV. (c) Corresponding power spectrum from a Fourier analysis. The frequency axis is displayed for beatings of Rydberg states with an energy spacing between 150 meV (27.6 fs) and 500 meV (8.3 fs). The main peak is at 291 meV (14.2 fs). The power spectrum of the experimental data of Fig. 2B is shown with a peak frequency at 264 meV (15.7 fs). (d) Calculated PECD for photoelectrons with $\epsilon = 500$ meV. (e) Corresponding power spectrum from a Fourier analysis with a central component at 269 meV (15.4 fs). The power spectrum of the experimental data of Fig. 2C is shown with a central frequency at ~329 meV (12.6 fs).

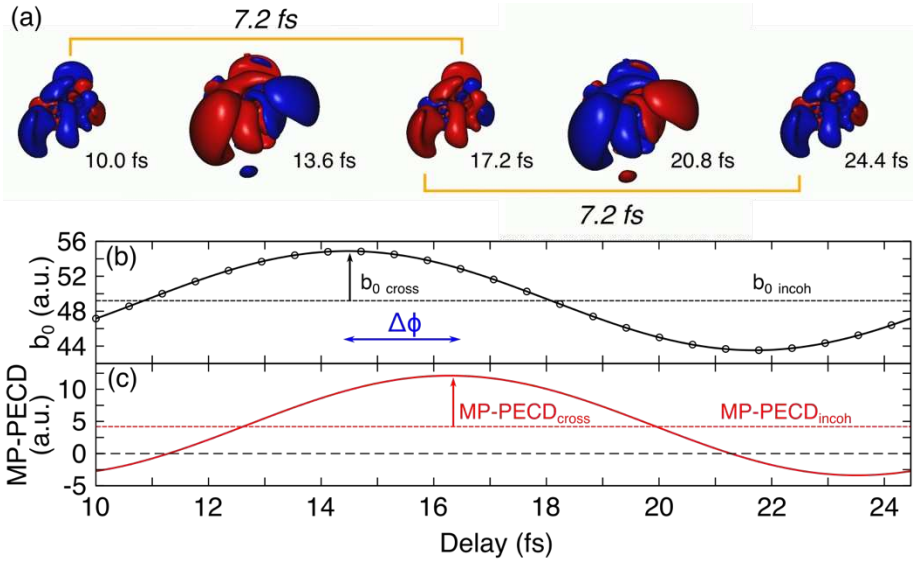


Fig. 4: **Electron-driven dynamics in the case of quantum beating monitored by 3d and 4p states**. (a) Temporal evolution of the coherent part of the electron density over one period of the quantum beating between the 3d and 4p states (see equation (1) of the text). (b) Photoelectron yield as a function of the pump-probe delay for $\epsilon = 250$ meV. The quantum beating leads to an oscillatory behavior of the yield which is in phase with the variation of the electron density shown in (a), as expected from equations (1) and (2). (c) MP-PECD as a function of the pump-probe delay for $\epsilon = 250$ meV. The dichroism is delayed by $\Delta\phi = 0.79$ rad (1.8 fs) with respect to the variation of the electron density because of the interferences between the continuum partial wave amplitudes (see equation (3)).